Received: 12 October 2022 | Revised: 5 May 2023 | Accepted: 10 July 2023

DOI: 10.1002/ajpa.24824

RESEARCH ARTICLE

AMERICAN JOURNAL OF BIOLOGICAL ANTHROPOLOGY

WILEY

Trabecular bone structure of the proximal capitate in extant hominids and fossil hominins with implications for midcarpal joint loading and the dart-thrower's motion

Emma E. Bird[1,2] | Tracy L. Kivell[1,3] | Christopher J. Dunmore[1] | Matthew W. Tocheri[4,5,6] | Matthew M. Skinner[1,3]

[1]Skeletal Biology Research Centre, School of Anthropology and Conservation, University of Kent, Canterbury, UK

[2]Centre for Human Evolution Research, Natural History Museum, London, UK

[3]Centre for the Exploration of the Deep Human Journey, University of the Witwatersrand, Johannesburg, South Africa

[4]Department of Anthropology, Lakehead University, Thunder Bay, Ontario, Canada

[5]Human Origins Program, National Museum of Natural History, Smithsonian Institution, Washington, DC, USA

[6]Australian Research Council, Centre of Excellence for Australian Biodiversity and Heritage, University of Wollongong, Wollongong, New South Wales, Australia

Correspondence
Emma E. Bird, Centre for Human Evolution Research, Natural History Museum, London, UK.
Email: emma.bird1@nhm.ac.uk

Funding information
FP7 European Research Council Starting Grant, Grant/Award Number: 336301; European Union's Horizon 2020 research and innovation programme, Grant/Award Number: 819960; ERC-SSHRC Visiting Scholar Program and SSHRC Insight Grant, Grant/Award Number: 435-2017-1234; The Max Planck Society; University of Kent; The Calleva Foundation

Abstract

Objectives: This research examines whether the distribution of trabecular bone in the proximal capitates of extant hominids, as well as several fossil hominin taxa, is associated with the oblique path of the midcarpal joint known as the dart-thrower's motion (DTM).

Materials and Methods: We analyzed proximal capitates from extant (*Pongo* $n = 12$; *Gorilla* $n = 11$; *Pan* $n = 10$; fossil and recent *Homo sapiens* $n = 29$) and extinct (*Australopithecus sediba* $n = 2$; *Homo naledi* $n = 1$; *Homo floresiensis* $n = 2$; Neandertals $n = 3$) hominids using a new canonical holistic morphometric analysis, which quantifies and visualizes the distribution of trabecular bone using relative bone volume as a fraction of total volume (rBV/TV).

Results: *Homo sapiens* and Neandertals had a continuous band of high rBV/TV that extended across the scaphoid, lunate, and hamate subarticular regions, but other fossil hominins and extant great apes did not. *A. sediba* expressed a distinct combination of human-like and *Pan*-like rBV/TV distribution. Both *H. floresiensis* and *H. naledi* had high rBV/TV on the ulnar-side of the capitate but low rBV/TV on the radial-side.

Conclusion: The proximal capitates of *H. sapiens* and Neandertals share a distinctive distribution of trabecular bone that suggests that these two species of *Homo* regularly load(ed) their midcarpal joints along the full extent of the oblique path of the DTM. The observed pattern in *A. sediba* suggests that human-like stress at the capito-scaphoid articular surface was combined with *Pan*-like wrist postures, whereas the patterns in *H. floresiensis* and *H. naledi* suggest their midcarpal joints were loaded differently from that of *H. sapiens* and Neandertals.

KEYWORDS
African apes, *Australopithecus*, cancellous bone, fossil *Homo*, wrist

In Honour of the Life and Scientific Contributions of Professor Mary Marzke

1 | INTRODUCTION

Among primates, carpal joint shapes and ranges of motion are associated with interspecific differences in hand use (Lewis, 1989; Marzke, 1997; Sarmiento, 1988). As such, the external form-function relationships of carpals have been crucial for developing an understanding of wrist function in extant hominids, including enabling assessments of arboreality and the capacity for tool behavior in fossil hominins (Lewis, 1989; Marzke, 1997; Marzke et al., 1992; Napier, 1962; Niewoehner et al., 1997; Orr et al., 2013; Tocheri et al., 2005). However, there are several limitations to inferences drawn from external form-function analyses. The external shape may not always reflect how the wrist was actually used as it may be influenced by factors that are not functionally significant (e.g., phylogenetic and/or developmental constraints) (Lieberman, 1997; Ward, 2002). Because of these limitations and the opportunity for more detailed hand and wrist functional inferences, recent studies have focused on analyzing the internal microarchitecture of trabecular (cancellous) bone (Barak et al., 2017; Matarazzo, 2015; Ragni, 2020; Tsegai et al., 2013). As trabecular bone is known to model aspects of its architectural properties in response to repeated loading (Barak et al., 2011; Pontzer et al., 2006), differences in the microarchitecture between individuals and taxa can be used to quantify variation in joint loading and behavior, as well as make more informed inferences about fossil hominin hand use.

Although it has been demonstrated *in vivo* that trabecular bone is actively modeled in response to novel changes in the loading environment (Barak et al., 2011; Pontzer et al., 2006), including in the tissues of adult *Homo sapiens* (Hughes et al., 2018), there are challenges and limitations to drawing behavioral inferences when applied to *ex vivo* research as in paleoanthropology (see Kivell, 2016). Nevertheless, a number of comparative analyses on phenotypically plastic aspects of bone have successfully linked certain aspects of trabecular bone microstructure to the expected forces associated with various primate behaviors (Barak et al., 2017; Chirchir et al., 2017; Fajardo & Müller, 2001; Griffin et al., 2010; Komza & Skinner, 2019; Ryan & Shaw, 2012; Tsegai et al., 2013). To date, these methods have been applied to a small number of fossil taxa to supplement and extend behavioral inferences drawn from external morphological analyses (Barak et al., 2013; Dunmore et al., 2020; Georgiou et al., 2020; Ryan & Ketcham, 2002; Skinner et al., 2015; Su & Carlson, 2017).

The first study of trabecular functional adaptation in the primate wrist failed to find support for several functional predictions (Schilling et al., 2014); however, the development of new 'whole-bone' techniques have yielded functionally meaningful results in this regard (Bird et al., 2021, 2022; Stephens et al., 2018). Stephens et al. (2018) found that the distribution of trabecular bone in the proximal capitate of recent humans coincided with its oblique range of motion across the scapho-lunate articular surface and therefore associated this pattern with the predicted kinematics of the dart-thrower's motion (DTM).

The DTM describes the natural motion of the human wrist (Crisco et al., 2005). The path of motion is oblique (i.e., out-of-anatomical plane) whereby the wrist moves from extension with radial deviation to flexion with ulnar deviation (Crisco et al., 2005). The proximal capitate is the central axis of rotation as it moves across an almost motionless proximal row (Crisco et al., 2005). The DTM is used for almost all activities of daily living, from maneuvering a screwdriver, pouring water from a jug, and turning a door handle, among many others (Figure 1a) (Brigstocke et al., 2014; Kaufman-Cohen et al., 2018). The geometry and congruence of the capitate-scapho-lunate joint are critical to the mechanics of the DTM (Figure 1b) (Edirisinghe et al., 2014; Garcia-Elias et al., 2014). Throughout movement, the loosely tethered lunate and scaphoid are continuously compacted tightly against one another, resulting in a congruent, stable scapho-lunate articulation for the capitate head (Garcia-Elias et al., 2014). Moreover, minimal muscle force is required to perform the DTM, and when the wrist is allowed to fall passively against gravity, extension or flexion is always accompanied by degrees of radial or ulnar deviation, respectively, suggesting that the intrinsic structures of the human wrist are highly adapted to the motion (Edirisinghe et al., 2014).

In practice, the DTM increases accuracy and velocity during hammering, clubbing, and throwing, as well as decreases the risk of injury from the resultant reaction forces (Williams et al., 2010, 2014; Wolfe et al., 2006). It has thus been hypothesized that it may have evolved as an adaptation to knapping activities (Williams et al., 2010; Wolfe et al., 2006). However, whether the DTM also characterizes the functional axis of the wrist in extant non-human hominids (*Pongo*, *Gorilla*, *Pan*) remains untested. Nonetheless, even if the DTM is widely shared among hominids, it is reasonable to expect that *H. sapiens* load the proximal capitate differently than other extant hominids because they do not regularly use their hands for locomotion (Marzke, 1997; Tocheri et al., 2008).

As trabecular bone patterning of the entire carpus has thus far only been mapped in *H. sapiens* (Stephens et al., 2018), the main objective of the present study is to quantify the distribution of trabecular bone volume in the proximal capitate in other extant hominids as well as various fossil hominins to determine whether they share the pattern that characterizes *H. sapiens*. To quantify and statistically compare the distributions of relative bone volume to total volume (rBV/TV) within the proximal capitate of these various taxa, we use microtomography and a novel 'whole-bone' canonical holistic morphometric analysis (cHMA), which combines statistical deformation modeling and holistic morphometric analysis (Bachmann et al., 2022; Steiner et al., 2021). Whole-bone methods allow us to quantify the distribution of bone throughout an entire region of interest (ROI), in this case, the proximal capitate. This contrasts with other methods, which have quantified bone by one (Ryan & Shaw, 2012; Schilling et al., 2014) or several (Barak et al., 2013; Chirchir et al., 2017; Dunmore et al., 2019) volumes of interest at the subarticular regions, but have typically not quantified the trabecular distribution deeper to the subarticular bone. The subarticular bone is assumed to contain the most intuitive and clear functional signals as it is closest to the origin of force (joint articulations); however, descriptions of the deeper trabeculae form an important component of the overall trabecular bone distribution pattern as force is transferred from the articular surface through the bone. Previously, Bird et al. (2021) quantified mean bone volume and degree of anisotropy across the proximal and distal

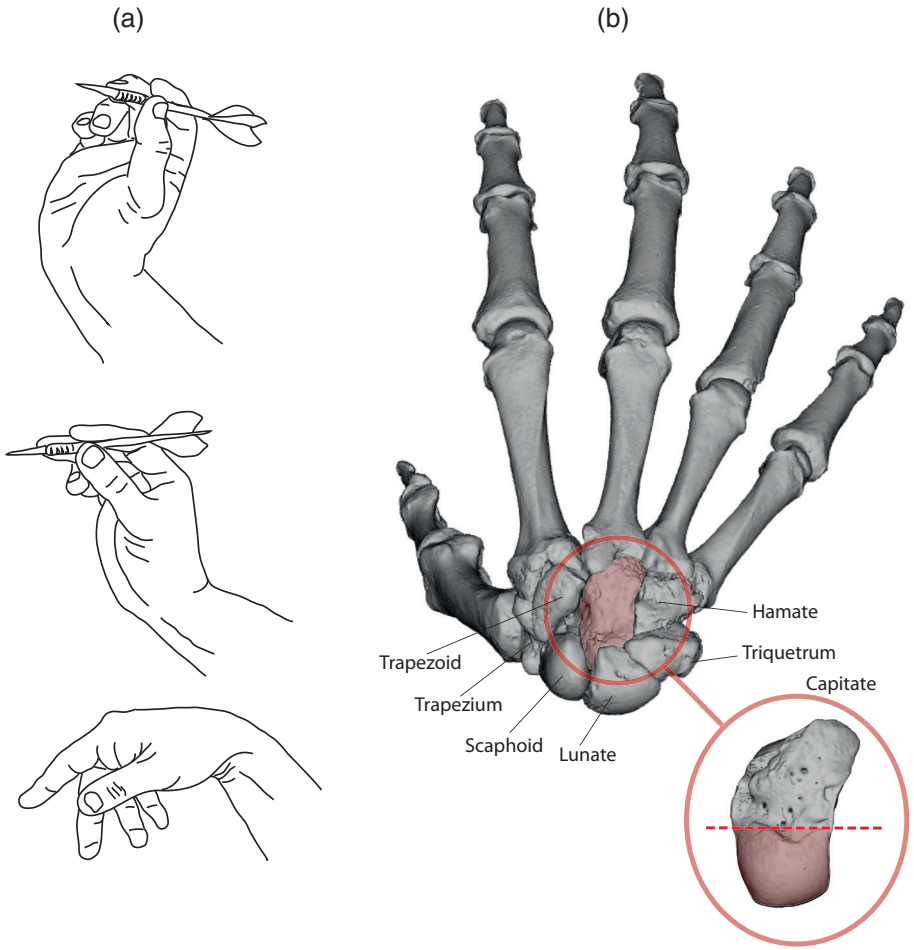

FIGURE 1 Anatomy and movement of the wrist in *H. sapiens*. (a) A hand moving through the dart-thrower's motion. (b) A *H. sapiens* right hand shows the position of the capitate (circled in red) in the center of the wrist. The capitate is also shown in isolation; the dotted line illustrates where the proximal capitate (colored in red) was separated from the distal capitate (colored gray).

segments of the capitate in extant hominids. While the trabecular microstructure differentiated extant hominids from one another, there was mixed support for the functional predictions, and trabecular bone distribution was not mapped (Bird et al., 2021). As such, it remains unclear whether the 'DTM pattern' identified by Stephens et al. (2018) is restricted to *H. sapiens* (and perhaps other hominins) and could be considered a signal of functional adaptation to habitual, human-like tool behavior.

Within our study, we predict that *H. sapiens* should show a similar trabecular distribution pattern as that found by Stephens et al. (2018), with a continuous radio-ulnar band of high rBV/TV at the subarticular scaphoid, lunate and hamate regions of the capitate. In contrast, capitates of extant non-human hominids should not show this pattern as their hands are routinely loaded during locomotion, which is hypothesized to load the midcarpal joint with greater force and in different postures compared to those of manipulative tasks (Lewis, 1989; Marzke, 1997; Richmond et al., 2001; Sarmiento, 1988). We also investigate the trabecular distribution patterns in capitates of Neandertals, *Homo floresiensis*, *Homo naledi*, and *Australopithecus sediba*. Although the precise wrist kinematics of tool behavior in these extinct taxa are uncertain, the current understanding of their anatomy and associated technology (or lack thereof) provides a baseline for what we can reasonably expect to see in their respective proximal capitate trabecular distribution patterns.

Like *H. sapiens*, Neandertals (~300–40 thousand years ago [ka]; Higham et al., 2014) are obligate tool users associated with Middle Paleolithic / Middle Stone Age technology and share a full suite of derived wrist features indicative of a functional commitment to precise and forceful gripping (Tocheri et al., 2008). As such, Neandertal capitates should show a pattern of trabecular distribution that is broadly similar if not identical to that seen in *H. sapiens*. Of the remaining three fossil species, only *H. floresiensis* (~100–60 ka) is directly associated with stone artifacts, all of which are best described as Oldowan-like technology (Brumm et al., 2006; Moore & Brumm, 2009; Sutikna et al., 2016). However, *H. floresiensis* retains several ancestral features in its wrist, including capitate shape (Orr et al., 2013; Tocheri et al., 2007). Thus, despite its primitive carpal morphology, we predict a trabecular bone distribution similar to that of humans, reflecting the habitual use of its hand for tool making and using.

Both *A. sediba* (1.977 million years ago (Ma) Pickering et al., 2011) and *H. naledi* (335–235 ka Dirks et al., 2017) exhibit morphological features associated with climbing and arboreality in the upper limb such as long, ape-like forelimbs for overhead reaching and curved manual phalanges for grasping (Churchill et al., 2013; Feuerriegel et al., 2017; Kivell et al., 2011; Kivell et al., 2018). Both species also exhibit a relatively long thumb capable of fully opposing the non-pollical digits; however, they vary in the degree of human-like manual

external morphology (Hawks et al., 2017; Kivell et al., 2015; Kivell et al., 2018). *A. sediba* has also demonstrated *Pongo*-like trabecular structure in the metacarpals alongside human-like trabecular structure in the thumb (Dunmore et al., 2020). An analysis of the capitate trabecular distributions in these South African taxa offers another line of evidence with which to investigate how these hominins used their hands. Given that *H. naledi* shares a suite of derived carpal and other hand features with *H. sapiens* and Neandertals (Hawks et al., 2017; Kivell et al., 2015), a human-like trabecular distribution in its capitate would suggest that this species used its hands in a similar way, providing indirect support that it may have made and used stone tools. The same can be said for *A. sediba*; however, given the more australopith-like shape of its capitate (Hawks et al., 2017; Kivell, 2015) and the recent trabecular evidence for climbing in the metacarpals (Dunmore et al., 2020,), we predict that it will display a pattern of trabecular distribution that is more similar to *Pongo*, reflecting habitual use of flexed finger postures.

2 | MATERIALS AND METHODS

2.1 | Sample

This study used micro-CT scans of left and right capitates from *Pongo* sp. ($n = 12$), *Gorilla* sp. ($n = 11$), *Pan* sp. ($n = 10$), and fossil and recent *H. sapiens* ($n = 29$) (Table 1). All specimens were adults with no signs of pathology. The extant non-human hominid samples are curated at various museums and represent individuals collected from the wild except for one zoo-housed orangutan. The recent human sample derives from spatio-temporally diverse populations (Chirchir et al., 2015; Stephens et al., 2018) (Supplementary Table 1). We also included three fossil *H. sapiens* from Late Pleistocene populations: Arene Candide 2 from 12 to 11 ka (Sparacello et al., 2018) and Barma Grande 2 from 17 to 15 ka (Formicola et al., 2004), both recovered in Western Liguria, Italy, as well as Ohalo 2 from 19 ka in Israel (Hershkovitz et al., 1995). Finally, the fossil hominin capitate sample includes three Neandertals from Israel: Tabun C1, 143 ± 37 ka (Coppa et al., 2005), Amud 1, 70–50 ka (Valladas et al., 1999), and Kebara 2, 60–50 ka (Schwarcz et al., 1989); two *H. floresiensis* (LB1-45 and LB20, both from Flores, Indonesia); one *H. naledi* (U.W. 101–1730, from the Rising Star cave system, South Africa); and one *A. sediba* (MH2, from Malapa, South Africa) represented by both the right (U.W. 88–156) and left (U.W. 88–105) sides.

TABLE 1 Summary of study sample categorized by sex and side.

Species	Sex	Side	
		Left	Right
Pongo abelii	Male		1
Pongo pygmaeus	Male	1	2
	Female	3	3
	Unknown	1	1
Gorilla gorilla	Male	1	6
	Female	2	2
Pan paniscus	Male		3
	Female	2	2
Pan troglodytes	Male	1	1
	Female	1	
Recent *Homo sapiens*	Male	6	6
	Female	1	4
	Unknown	8	4
Pleistocene *Homo sapiens*	Male	2	1
Neandertal	Male	2	
	Female	1	
Australopithecus sediba	Female	1	1
Homo naledi	Unknown		1
Homo floresiensis	Female	1	1

2.2 | Data collection

Specimens were micro-CT scanned either at the Max Planck Institute for Evolutionary Anthropology, Leipzig, Germany using a BIR ACTIS 225/300 or Diondo D3, or at the University of Cambridge Biotomography Centre, Cambridge, UK using a Nikon 225/XTH. Scans used a 0.2–0.5 mm copper or brass filter at an acceleration voltage of 100–160 kV and 100–140 μA. To ensure that thin trabecular struts were accurately measured, isometric scan resolution was between 0.02 and 0.03 mm (Supplementary Table 1). Images were reconstructed as 16-bit volumetric tiff stacks. Using Avizo 6.3 or 9 (Visualization Sciences Group, SAS), surface models were oriented into a standard anatomical position, and left capitates were mirrored to orient them with rights. The medical imaging analysis (MIA) clustering method was used to remove non-bone material from the scans and produce a binary segmentation of bone and non-bone material (Dunmore et al., 2018). All fossil segmentations were performed by one author (Emma E. Bird), and reviewed by co-authors (Christopher J. Dunmore, Tracy L. Kivell, Matthew M. Skinner). Image segmentations were then tissue segmented into cortical and trabecular bone in medtool 4.3 (http://www.dr-pahr.at/medtool/). By projecting a series of mathematical rays across the scan, medtool 4.3 assigns unique scalars to the trabecular, cortical, internal air, and background voxels (Gross et al., 2014; Tsegai et al., 2013). The trabecular and cortical bone elements were then separated so that trabecular bone could be analyzed independently.

The cHMA protocol uses a statistical deformation model to create a canonical shape that can be morphed to all capitates in the sample in 3D space (Bachmann et al., 2022; Steiner et al., 2021). Briefly, two iterations of a similarity and b-spline registration were run on each capitate. The registration process results in a solid canonical capitate trabecular volume, representing the mean size, shape, and position of the internal trabecular bone space of the entire sample (for a visual representation of the method, see Bachmann et al., 2022). The canonical model was then meshed and morphed to individual trabecular

volumes using the transformation data from the statistical deformation model. Holistic morphometric analysis was then run in medtool 4.3 to quantify bone volume fraction (BV/TV) (Gross et al., 2014; Tsegai et al., 2013). In short, a 3D grid with nodes spaced 2.5 mm apart was placed over each individual trabecular volume. A 5 mm sampling sphere was centered on one node and then moved from node to node, iteratively measuring trabecular BV/TV. These BV/TV values were interpolated onto each morphed canonical mesh, which could then be morphed back to its canonical shape while retaining individual BV/TV distributions. Color maps representing the distribution of BV/TV were viewed in Paraview (v3.98) (http://www.kitware.com/products/paraview.html). Since data were collected on the canonical mesh, the tetrahedra of this mesh are homologous among individuals. Next, using Paraview (v.3.98), the canonical mesh was split into a proximal and distal part so that the proximal capitate could be analyzed separately. The separation was made at the distal extent of the lunate articular surface, as per Bird et al. (2021). Finally, the BV/TV of each tetrahedron was divided by the average BV/TV of all tetrahedra in each individual to produce a dataset representing rBV/TV. Where absolute, or baseline, bone volume may reflect both functional and systemic signals, or a mixture of these (Chirchir et al., 2015; Tsegai et al., 2018), rBV/TV demonstrates where bone volume has increased or decreased relative to the mean. Here we assume regions of high rBV/TV reflect the positions in which joints are frequently and substantially loaded.

2.3 | Statistics

The mean rBV/TV distributions for each extant taxon, the Pleistocene *H. sapiens*, and Neandertal samples were calculated by arithmetically averaging the rBV/TV of the individuals in each group at each homologous tetrahedron. Each taxon-specific distribution was then mapped to the canonical mesh and visualized in Paraview (v3.98). The total rBV/TV dataset was further explored using principal component analysis (PCA) in R Statistical Software (v4.1.0; R Core R Core Team, 2013). The first three PCs were visualized in 2D using the factoextra R package (v1.0.7; Kassambara & Mundt, 2020) and 3D using the plot3d R package (v1.4; Soetaert, 2021). Loadings representing three signed standard deviations of each principal component (PC) were mapped to the canonical mesh situated at the positive and negative ends of each axis. Using these loadings, a capitate model was built to visualize the extreme patterns of rBV/TV driving variance along the axes. These loadings were also thresholded at the 60th percentile of their maximum rBV/TV range allowing volumetric visualization of the capitate regions that most strongly drive the variation observed along each PC. To test for group differences among the extant taxa, a one-way permutational MANOVA was conducted using the first three PC scores (which explained the majority of the sample variance) in the vegan R package (v2.5-7; Oksanen et al., 2021). If this test was statistically significant, pairwise one-way permutational MANOVAs were then run using a Bonferroni correction in the RVAideMemoire R package (v0.9-80; Hervé, 2021).

3 | RESULTS

3.1 | Extant taxa

Figure 2 illustrates the mean rBV/TV distribution of each extant taxon (see Supplementary Figure 1 for the standard deviations around this mean and Supplementary Figure 2 for individual rBV/TV maps and two cross-sections of the original trabecular structure). Individual BV/TV values are provided in Supplementary Table 1 and a qualitative description of the taxon-specific mean rBV/TV distribution is given in Supplementary Table 2. The qualitative descriptions of rBV/TV distributions are summarized below and include a description of rBV/TV at the subarticular trabeculae as well as within the deeper trabecular structure (i.e., deep to the subarticular bone). Taxon-specific mean rBV/TV distributions are visualized in color maps (Figure 2).

Recent *H. sapiens* was characterized by a continuous band of high rBV/TV at the subarticular region of the scaphoid, lunate and hamate (Figure 2). Although the rBV/TV was typically high across the entire radio-ulnar portion of the capitate head, the highest values were typically on the lunate subarticular region (Figure 2, proximal view). This high rBV/TV extended from the subarticular trabeculae through the capitate distally (Figure 2, sagittal cross-section). In *Pan*, high rBV/TV occurred at the lunate articular surface and extended ulnarly onto the hamate surface but not radially onto the scaphoid surface, which had moderate rBV/TV (Figure 2, proximal and radial views). *Pan* was the only extant genus to typically show high rBV/TV on the palmar non-articular surface that continued ulnarly onto the hamate facet (Figure 2, palmar view). The sagittal cross-section in Figure 2 shows high rBV/TV on the palmar and ulnar sides, extending through the center of the capitate, creating a continuous disto-palmar band of high rBV/TV within the deeper trabecular structure (i.e., non-subarticular trabeculae). *Gorilla* was characterized by high rBV/TV at the ulnar and radial sides of the head, but these regions did not form a continuous band across the capitate head, as moderate rBV/TV was seen at the proximal scaphoid subarticular area (Figure 2, proximal view). High rBV/TV occurred at the subarticular trabeculae only and did not extend into the deeper trabeculae (Figure 2, sagittal cross-section). Finally, *Pongo* was characterized by moderate rBV/TV at the lunate articular surface and low rBV/TV at the scaphoid subarticular region (Figure 2, proximal and radial views). Moderate rBV/TV continued distally, with increased rBV/TV in the deeper trabeculae, and the highest rBV/TV seen in the central and distal components of the capitate head (Figure 2, sagittal cross-section). The zoo-housed individual does not show any obvious deviation from this pattern.

The MANOVA indicated that there was a statistically significant difference among the extant hominid distributions of rBV/TV ($p < 0.001$) and all post-hoc permutational pairwise Bonferroni-corrected comparisons were also significantly different ($p < 0.001$; Table 2). The PCA illustrates the variance in rBV/TV distribution (Figure 3). PC1 explained 29.5% of the variance and generally separated *H. sapiens* (positive PC1 scores) from *Pongo* and *Pan*, with *Gorilla* falling almost exactly at the intersection of PC1 and PC2. Positive PC1 scores correlate with high rBV/TV across the proximal-most capitate,

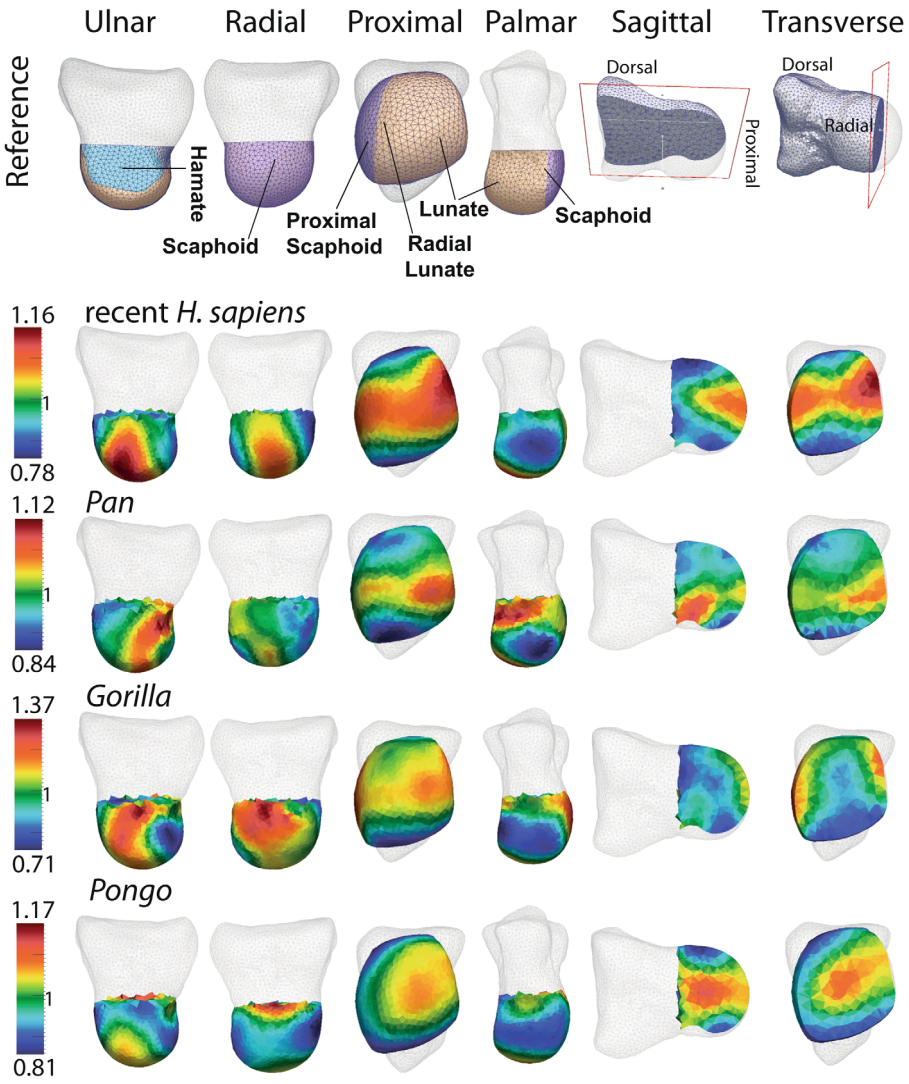

FIGURE 2 Mean relative bone volume to total volume (rBV/TV) distribution maps in the capitate head of each extant taxon. The first four columns of the reference images illustrate the subarticular regions of the proximal capitate. The last two columns of the reference images illustrate where a slice has been placed in the canonical model to show the internal structure. The mean rBV/TV value for each taxon is represented by green (1). Warmer colors represent higher than average bone volume, and cooler colors represent lower than average.

TABLE 2 Results of the post-hoc, permutational multivariate pairwise comparisons of extant hominins.

	Gorilla	*H. sapiens*	*Pan*
H. sapiens	<0.001	/	/
Pan	0.001	0.001	/
Pongo	<0.001	<0.001	<0.001

extending radially, ulnarly, and distally (Figure 3a). Negative PC1 scores correlate with high rBV/TV in the palmar portion of the distal-most aspect of the capitate head, as typically seen in *Pan* (Figure 2). PC2 explained 14.6% of the variance, where only *Gorilla* had a mean score substantially above 0. Positive PC2 scores are driven by high rBV/TV at the subarticular disto-dorsal and radial surfaces. Negative PC2 scores correlate with high rBV/TV at the subarticular lunate as well as proximal hamate and scaphoid articular surfaces, which extend distally through the capitate head. PC3 explained 10.2% of the variance and generally separated *Pongo* and *H. sapiens* (positive PC3 scores) from African apes. Positive PC3 values correlate with high rBV/TV in the center of the distal-most portion of the head, as typical in *Pongo* (Figure 2). Negative PC3 values correlate with high rBV/TV at the subarticular trabeculae at the scaphoid, lunate, and hamate surfaces, extending towards the palmar surface.

3.2 | Fossil hominins

Figure 4 illustrates the mean rBV/TV distribution patterns for Pleistocene *H. sapiens* and Neandertals (see Supplementary Figure 2 for individual maps), as well as individual capitate maps for the left and right *A. sediba*, *H. floresiensis*, and *H. naledi*. The rBV/TV distributions in Ohalo 2 and Barma Grande 2 resembled the typical recent *H. sapiens* pattern, although Arene Candide 2 had lower rBV/TV at the scaphoid subarticular region and higher rBV/TV at the proximo-palmar lunate region. In the PCA, Barma Grande 2 plotted within the range of recent *H. sapiens*, whereas Ohalo 2 and Arene Candide 2 plotted close to, but outside, this range due to negative PC2 values driven by the dorso-palmar expansion of the high subarticular rBV/TV on the proximal-most portion of the head. In Neandertals, Kebara

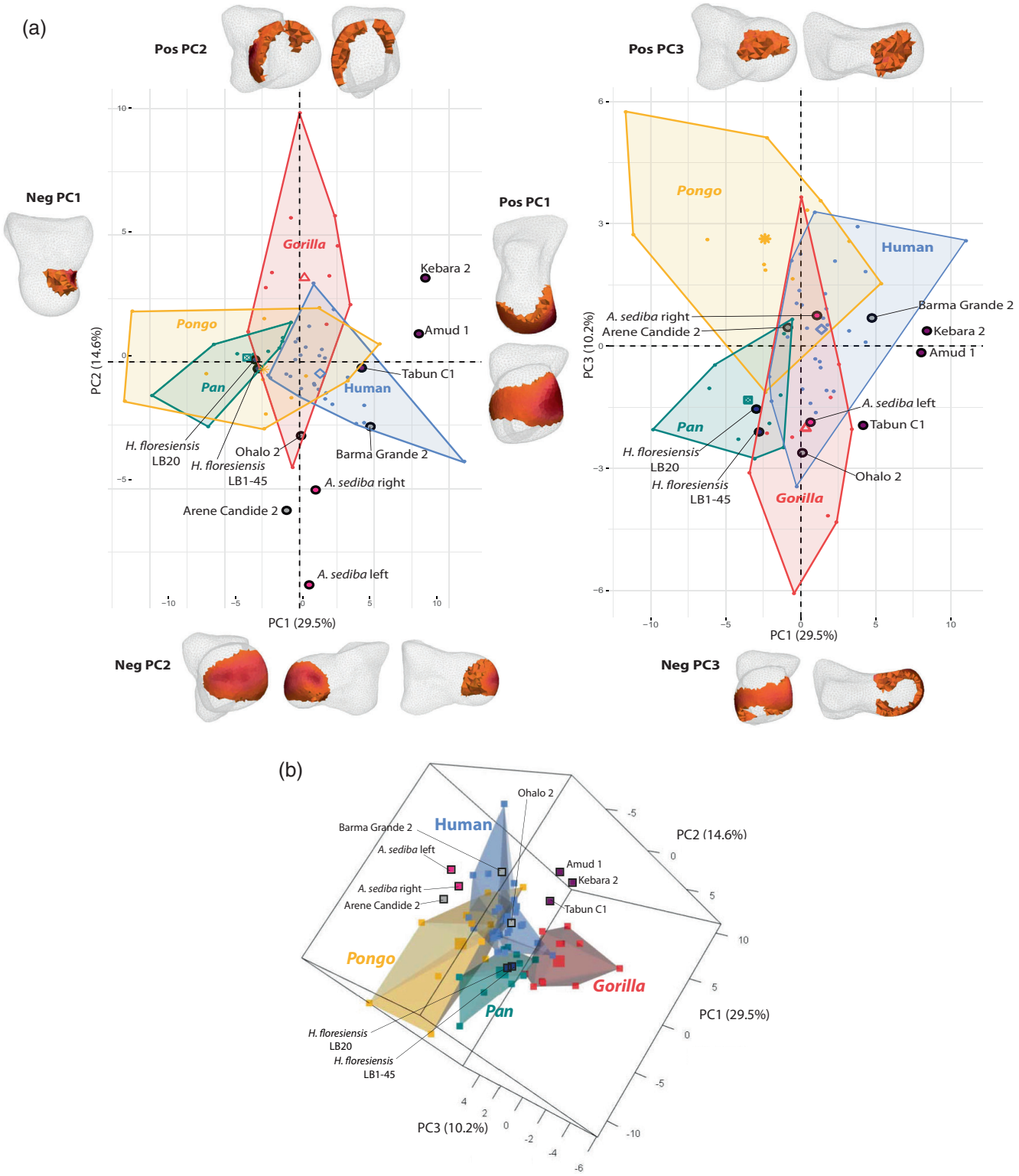

FIGURE 3 Results of the principal component analysis (PCA) analysis. (a) PC1 and 2 (left), and PC2 and 3 (right). Models at the end of each axis represent the regions of high rBV/TV (in red) driving variance along those PCs. (b) PCA showing the separation in 3D space. Fossils are labeled individually in both figures.

2 and Tabun C1 both exhibit the two defining features of the recent *H. sapiens* distribution, while Amud 1 exhibited slightly lower rBV/TV at the scaphoid subarticular region. All three Neandertals sampled plotted close to one another, but Kebara 2 and Amud 1 fell outside the recent human morphospace primarily due to higher scores along positive PC1.

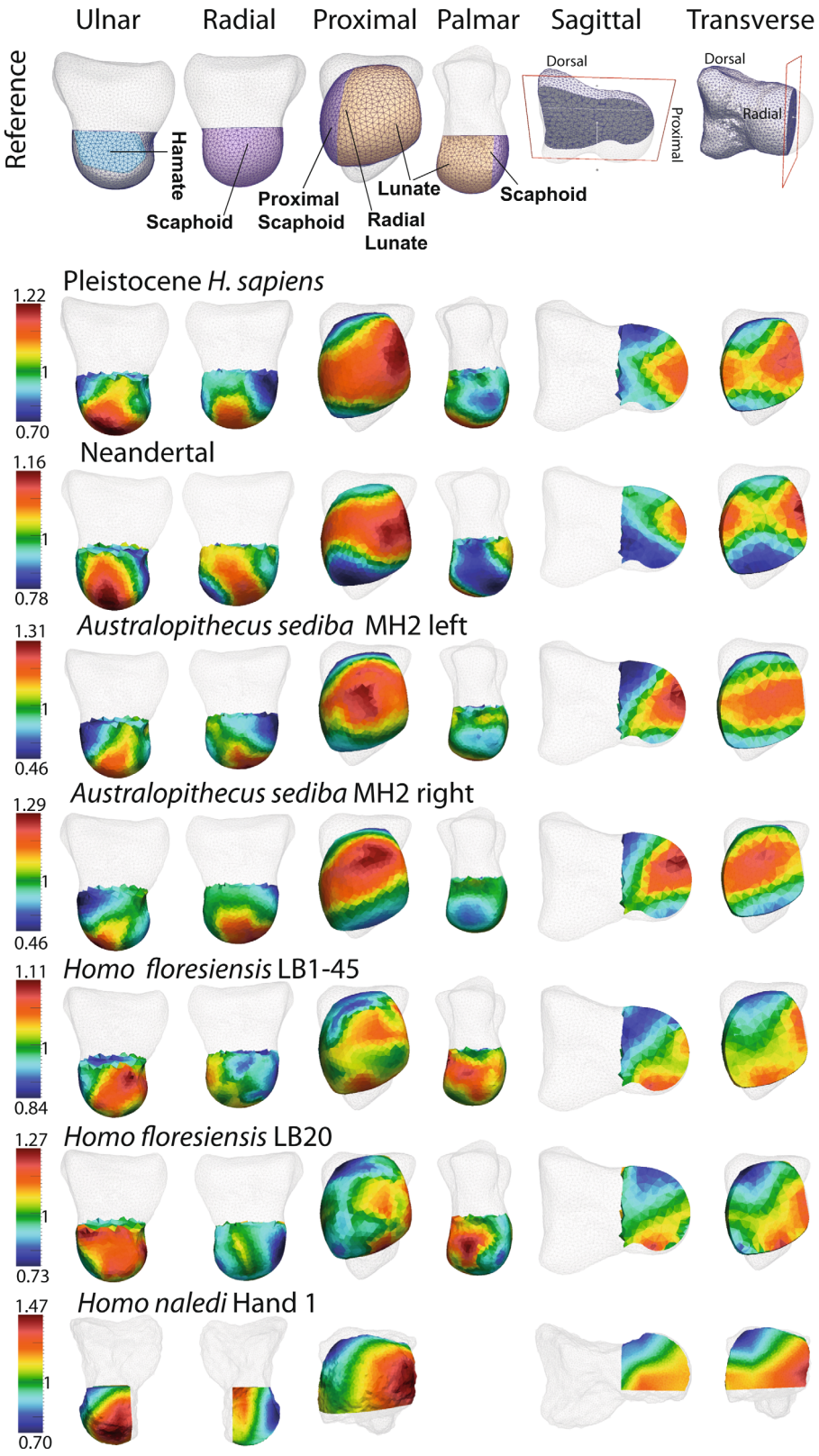

FIGURE 4 Relative bone volume to total volume (rBV/TV) distribution maps in the capitate head of the fossil sample. Fossil *H. sapiens* and Neandertals are represented by a mean map, *A. sediba*, *H. naledi*, and *H. floresiensis* are represented individually. In the reference image, the first four images illustrate the articular surfaces of the proximal capitate, and the last two illustrate where a slice has been placed in the canonical model to show the internal rBV/TV. The mean rBV/TV value for each taxon is represented by green (1). Warmer colors represent higher than average bone volume, and cooler colors represent lower than average. *H. naledi* Hand 1 is represented on its actual shape as the broken palmar portion excluded it from statistical analysis. The broken element has been removed from the visualization. High-resolution images of the bone, including the extent of the damage, can be seen in Kivell et al. (2015).

Both the right and left *A. sediba* capitates plotted positively on PC1 and negatively on PC2, outside the range of any extant hominid. Both bones showed a distinct radio-ulnar band of high rBV/TV distribution that did not extend as far distally on the radial and ulnar sides as was typically seen in *H. sapiens* and Neandertals. The subarticular band of high rBV/TV extended disto-palmarly through the trabeculae, distinguishing it from the predominantly distal orientation in *H. sapiens* and Neandertals. While *Pan* also showed a disto-palmar

orientation of high rBV/TV, it only originated proximally, while in *A. sediba* it originated proximally and radially. Both right and left bones fell at around the same position on PC1 but were separated along PC2 and PC3. MH2 left has a higher score along negative PC2 than the right due to the relatively expanded dorso-palmarly height of the high rBV/TV at the proximal subarticular region. Along PC3, the left capitate fell on the negative axis and the right fell on the positive. This is due to the left capitate having a greater distal extension of high rBV/TV on the hamate subarticular region. In the right capitate, high rBV/TV within the deeper trabeculae and relatively lower rBV/TV in the hamate subarticular region is driving its variance to positive PC3.

The *H. floresiensis* capitates plotted close to one another on the PCA, very near to the *Pan* centroid (Figure 3). Both capitates had high rBV/TV on the palmar surface, and lunate and hamate subarticular regions (Figure 4). Both bones were clearly distinguished from the typical *H. sapiens* and Neandertal pattern as neither expressed high rBV/TV at the scaphoid subarticular region nor a band of distally oriented high rBV/TV within the deeper trabeculae. This rBV/TV pattern aligns *H. floresiensis* mostly with *Pan* as it is the only extant taxon to typically show both high rBV/TV at the palmar region (Figure 2) and higher rBV/TV at the ulnar side relative to the radial side of the capitate.

Due to the fragmented region on the palmar portion of the *H. naledi* capitate, this specimen was not included in the PCA, and the distribution of rBV/TV was only analyzed on its preserved shape (Figure 4). It showed several similarities with the typical *Pan* pattern, including high rBV/TV at the capito-lunate and capito-hamate joints, although its distribution was dorso-palmarly taller than was typical of *Pan*. The high rBV/TV at the lunate surface did not extend radially onto the scaphoid articular surface, clearly differentiating *H. naledi* from the typical *H. sapiens*-Neandertal pattern. The disto-radial portion of the scaphoid also expressed higher rBV/TV values, somewhat resembling the typical *Gorilla* pattern (Figure 2). Again, similar to *Pan*, high rBV/TV was concentrated on the ulnar side of the bone and appeared to extend towards the palmar aspect. However, as this region was broken in *H. naledi*, it must be interpreted cautiously.

4 | DISCUSSION

4.1 | Extant taxa

Prior to this study, the distribution of trabecular volume in hominid carpal bones had only been mapped in *H. sapiens* (Stephens et al., 2018) and our study addressed this gap by quantifying rBV/TV in proximal capitates of other extant hominids and several fossil hominins. We demonstrated that the mean distribution of proximal capitate rBV/TV in recent *H. sapiens* significantly differs from that of other extant hominids. Specifically, two features appeared consistently among our recent *H. sapiens* sample: first, and in line with our predictions, no other extant species consistently expressed a continuous radio-ulnar band of high rBV/TV across the capitate head incorporating the scaphoid, lunate and hamate subarticular regions; second, the distal extension of high rBV/TV into the body of the capitate distinguished recent humans from *Pan*, *Gorilla*, and *Pongo*, as only in recent humans did this band originate from both the scaphoid and lunate subarticular regions. This suggests that recent *H. sapiens* load the capito-lunate, capito-scaphoid and capito-hamate articular surfaces similarly, although the capito-lunate joint tended to have the absolute highest rBV/TV values across the whole proximal capitate. Similar to *H. sapiens*, rBV/TV was higher at the lunate subarticular region relative to the proximal scaphoid in non-human hominids. Most likely, this is due to the fact that the capito-lunate joint in non-human hominids is under regular loading during locomotor behaviors.

Like recent *H. sapiens*, the mean rBV/TV distributions for *Gorilla* and *Pan* proximal capitates showed higher concentrations of rBV/TV radio-ulnarly across the capitate head (Figure 2, proximal view). However, unlike in *H. sapiens*, this high concentration rBV/TV was not a continuous band as rBV/TV was only somewhat concentrated at the radial portion of the lunate and proximal portion of the scaphoid subarticular regions in *Pan* and *Gorilla* (Figure 2, proximal view). Nevertheless, the similarity between the hominine taxa is particularly evident when compared to *Pongo*, which showed low rBV/TV at the radial lunate and scaphoid subarticular regions. The distinctive pattern in *Pongo* is consistent with functional interpretations that have suggested the dorso-palmarly tall and radio-ulnarly wide lunate plays a central role in force transfer between the fingers and forearm, particularly *in lieu* of a fully-developed triangular fibrocartilaginous complex to facilitate force transfer between the triquetrum and ulna (Lewis, 1989; Sarmiento, 1988). Furthermore, the screw-clamp mechanism of the *Pongo* midcarpal joint is not as effective as in African apes. The screw-clamp mechanism describes how the midcarpal complex reaches a closed-pack position at low-levels of wrist extension, which is hypothesized to provide stability to the wrist for weight-bearing during locomotion (Lewis, 1989; Orr, 2017). Compared to *Pan* or *Gorilla*, *Pongo* shows a higher degree of wrist extension before the capitate and scaphoid reach full congruence (Orr, 2017) and thus loading may be distributed across a wider region of the radio-proximal capitate. Conversely, the hominine pattern may reflect a shared feature of greater radial-wrist stability through an axis of movement at the midcarpal joint that results in greater load bearing through a smaller portion of the capito-scaphoid articular surface. Greater radial-side wrist loading has been hypothesized to be associated with the knuckle-walking postures used by the African apes (Jenkins & Fleagle, 1975; Orr, 2017; Richmond et al., 2001).

Despite these similarities, *Pan* and *Gorilla* rBV/TV patterns were significantly different from each other (Table 2). In *Gorilla*, the rBV/TV distribution suggested high load was experienced relatively evenly at the subarticular scaphoid and hamate regions, while in *Pan* loading appeared to be relatively higher at the hamate and lunate regions. Moreover, areas of high rBV/TV in *Gorilla* did not extend below the subarticular bone into the center of the capitate head (Figure 2, sagittal and transverse view), whereas *Pan* had a distinctive band of high rBV/TV, oriented disto-palmarly through the capitate. Among extant hominid proximal capitates, *Gorilla* shows the greatest mean cortical

bone thickness (Bird et al., 2021), which potentially provides the necessary stiffness for resisting deformation from loading without the need of increased trabecular bone density beneath the subarticular bone. However, mean cortical thickness is also substantial in *Pan* (Bird et al., 2021), which did have a distal extension of high rBV/TV from the subarticular bone. Overall, the *Pan* pattern suggests loading at the lunate and hamate joints were higher than at the capito-scaphoid joint. The differences between the two African apes may be linked to variable use of ulnar deviation, which is thought to be high during climbing and the palm-in knuckle-walking postures frequently adopted by *Pan* (Matarazzo, 2013; Thompson, 2020; Tuttle, 1967; Wunderlich & Jungers, 2009 but see Samuel et al., 2018). Although *Gorilla* uses higher degrees of ulnar deviation during vertical climbing (Neufuss et al., 2017), this behavior is performed at lower frequencies than knuckle-walking in both taxa (Doran, 1996). The locomotor repertoire of the African apes is varied and is correlated with several ecological (Doran & Hunt, 1994; Neufuss et al., 2017; Remis, 1999) and life history factors (Doran, 1996). While the homology of knuckle-walking between the two taxa is debated (Dainton & Macho, 1999; Kivell & Schmitt, 2009; Richmond et al., 2001), our results suggest that the locomotor differences between the two African apes are reflected in their underlying proximal capitate rBV/TV distributions. Although previous studies of *Pan* carpals found no statistically significant differences in mean trabecular parameters between *P. troglodytes* and *P. paniscus* (Bird et al., 2021, 2022), further examination of rBV/TV distribution in the carpals of these species is warranted, and may provide more insight into the differences observed between *Gorilla* and *Pan* in the current study.

4.2 | Fossil hominins

The proximal capitates of Pleistocene *H. sapiens* and Neandertals broadly shared a similar pattern of trabecular bone distribution as recent *H. sapiens*. Therefore, our results support and extend upon the findings of Stephens et al. (2018), suggesting that *H. sapiens* and Neandertal proximal capitates display a distinctive, continuous radio-ulnar band of high rBV/TV, which reasonably tracks the oblique path of the DTM. These results thus suggest that despite behavioral variation across these two taxa, Neandertals likely habitually loaded their midcarpal joints along the full extent of the DTM in similar ways to that of *H. sapiens*. Neandertals clustered together along PC1 expressing the highest values on the PC, suggesting there was consistent and heavy loading across the DTM axis with little variation among the sample (albeit the Neandertal sample size is relatively small). Other studies have found differences in the microarchitecture and muscle markings of the hand bones of these two taxa (Bardo et al., 2020; Dunmore et al., 2020; Karakostis et al., 2018; Niewoehner et al., 1997), but our results are consistent with the radial wrist and carpometacarpal joint geometry, which suggests similar dexterity and manipulative capacities between the two taxa (Marzke, 2013; Tocheri et al., 2008).

Differences between *H. sapiens* and Neandertals (or between *H. sapiens* populations) may occur within other functional units of the wrist. While the DTM kinematics are compatible with transverse power grips (holding something large), a power squeeze grip (holding a hammer/handle) and precision grips (holding a), these behaviors may load the more distal elements of the hand differently. For example, transverse power grips likely induce greater loading of the wrist ulnarly compared to precision grips (Marzke et al., 1992; Niewoehner et al., 1997). Therefore, examining rBV/TV in the bones of the distal carpal row is warranted (i.e., the distal capitate rather than the proximal capitate). Accurate interpretations of rBV/TV differences in the wrists (including some of the variation seen within the results of this study) of *H. sapiens* and Neandertals will likely require a greater understanding of wrist postures across variable tool use behaviors. For instance, wrist flexion is rarely used during stone tool manufacture (Williams et al., 2010, 2014; Williams-Hatala et al., 2021), although it is used for scraping during hide preparation (Key et al., 2020). Interestingly, Arene Candide 2 had higher rBV/TV in the palmar aspect of their proximal capitate than was typical for our recent *H. sapiens* sample, possibly indicating frequent use of wrist flexion, as the lunate and palmar capitate head are congruent in this posture (Edirisinghe et al., 2014). Although posture during tool manufacture has been quantified in some studies (Key et al., 2018; Key et al., 2019; Key et al., 2020; Williams et al., 2010, 2014; Williams-Hatala et al., 2021), currently it is challenging to relate variation within our recent human and Neandertal sample to specific behaviors.

Although our results support the hypothesis that the rBV/TV distribution in *H. sapiens* and Neandertals reflects habitual use of the DTM, it is important to remember that high rBV/TV is not *ipso facto* evidence of bone kinematics (i.e., intercarpal motion). The human scapho-capitate articular surface is relatively larger than in non-human hominids, which is considered an adaptation to high forces arising from the thumb during tool behaviors (Tocheri et al., 2008). Thus, high rBV/TV at the capito-scaphoid subarticular region may also be reasonably linked to the forces incurred via forceful, manipulative behaviors; that is to say, the pattern may reflect the kinetics of forceful precision gripping rather than midcarpal movement alone. Furthermore, it is important to note that these results do not imply the DTM is a wrist movement unique to *H. sapiens* and Neandertals. This study assumes that high rBV/TV reflects peak, habitual loading magnitudes, and so it remains a possibility that non-human hominids are using the DTM for manipulative tasks, but at a magnitude or frequency that does not illicit bone modeling. In light of this, important directions for future study include whether rBV/TV distribution in *H. sapiens* and Neandertals is: (1) a reflection of high capito-scaphoid strain from a primarily manipulative thumb in combination with high capito-lunate strain as a shared feature of hominid wrist kinetics or (2) a result of habitual movement across the DTM axis of the midcarpal joint. Moreover, quantifying intercarpal motion in non-human hominids during object manipulation and tool use is essential comparative data necessary for understanding the evolution of the DTM. Nevertheless, our results suggest that the strains induced at the proximal capitate in the primarily manipulative hand of recent and Pleistocene *H. sapiens* as well as Neandertals are clearly distinct from those of extant non-human hominids, which habitually use their hands during locomotion. These novel

comparative data offer a new opportunity to assess how other extinct hominin species may have used their hands.

The distributions of rBV/TV in the two *A. sediba* capitates (MH2) expressed a distinct combination of features. Our prediction that *A. sediba* would most closely resemble the *Pongo* trabecular bone distribution pattern is therefore not supported. The subarticular bone resembled the pattern of *H. sapiens* and Neandertals, suggesting that *A. sediba* heavily and consistently loaded the proximal capitate at least across the middle portion of the DTM axis; however, the disto-palmar extension of high rBV/TV from the capito-scaphoid and capito-lunate subarticular regions more closely resembles the pattern in *Pan*. This latter feature suggests wrist postures during peak loading in *A. sediba* were distinctive from that of *H. sapiens* and Neandertals. In *Pan* and *A. sediba*, disto-palmarly oriented strain through the proximal capitate may reflect loading during ulnarly deviated hand postures. Many aspects of the *A. sediba* wrist, hand and upper limb (Churchill et al., 2013; Kivell et al., 2011; Kivell et al., 2018) and lower limb (DeSilva et al., 2018) morphology suggest arboreality was still a significant component of its positional repertoire, and dental calculus and wear patterns suggest a *Pan*-like diet high in fruit, bark, and leaves (Henry et al., 2012). Moreover, a comparative study of the subarticular trabecular rBV/TV distribution of the metacarpals in *A. sediba* found patterns of functional adaptation consistent with significant proportions of both flexed power grasping for arboreality and human-like manipulation with the thumb (Dunmore et al., 2020). In *A. sediba*, the thumb is long relative to the fingers, which suggests a capacity for pad-to-pad precision grips, while the asymmetrical metacarpal heads likely allowed thumb and fifth finger adduction for increased grip stability and precision (Kivell et al., 2011; Kivell et al., 2018; Marzke, 1997; Napier, 1962; Tocheri et al., 2008). Although the kinetics and kinematics of the midcarpal joint in *A. sediba* most likely were different than in *H. sapiens* and Neandertals, our results are consistent with previous interpretations that *A. sediba* regularly loaded its thumb during manipulative behaviors, but otherwise did this while utilizing more *Pan*-like wrist postures.

Although an in-depth discussion of lateralization is outside the scope of this paper, it is notable that the MH2 capitates were separated along PC2 and PC3. Although *H. sapiens* overwhelmingly exhibit a right-handedness bias, clinical literature indicates that the midcarpal joint uses the DTM in both the dominant and non-dominant hand across a wide range of activities (Kaufman-Cohen et al., 2018). Furthermore, Reina et al. (2017) found that although measured grip strength was higher in the dominant hand, this did not translate to statistical differences in the trabecular architecture of the carpus between the dominant and non-dominate hands. Thus, even though the role of the hands is often differentiated, it appears reasonable to assume rBV/TV distribution would be similar in the midcarpal joint of the right and left hands. Both right and left MH2 capitates fell at a similar position along PC1, which is reflected in their shared human-like distribution of rBV/TV at the lunate and scaphoid subarticular regions. Nevertheless, the observed differences between the two bones is interesting and suggest that further investigation of lateralization patterns in capitate trabeculae within a larger comparative sample are warranted.

Both *H. floresiensis* capitates (LB1-45 and LB20) clustered closely to the *Pan* centroid in the PCA, primarily due to high rBV/TV at the ulnar and palmar aspects of the capitate head. This rBV/TV distribution pattern suggests that *H. floresiensis* made Oldowan-like tools without using typical human-like loading of the midcarpal joint and therefore did not support our prediction. The inherent flexibility of the hominid hand means it is challenging to precisely infer the grips used by fossil hominins based on their external wrist morphology; however, the abundance of stone tools, in combination with the well-developed soft tissue attachments on the thumb (Larson et al., 2009), suggests that *H. floresiensis* was using some kind of forceful, precision gripping (Orr et al., 2013). A relatively robust and slightly distally projecting hamate hamulus suggests that *H. floresiensis* may have had a mechanical advantage for loading the ulnar aspect of the hand as it potentially indicates hypertrophied musculature as well as more powerful flexion and ulnar deviation at the wrist (Orr et al., 2013). Emphasis on high loading of the ulnar-side digits has been correlated to transverse-type grips such as the cradle grip (Key et al., 2019; Niewoehner et al., 1997; Williams-Hatala et al., 2021), which is one of the main postures used by novice stone knappers when making Oldowan tools in modern experiments (Key et al., 2018;Marzke, 1997; Williams-Hatala et al., 2021). Higher rBV/TV on the ulnar-side of the *H. floresiensis* capitate heads suggests the use of transverse-type grips as relatively high loading from the fourth and fifth digits would be transferred to the proximal capitate via the hamate. Further, the ape-like radial carpal joint configurations would have been well-adapted to resist proximo-distally oriented force vectors from the ulnar-side digits during these grips (Marzke, 1997; Niewoehner et al., 1997; Orr et al., 2013).

Locomotion that uses the forelimb, such as climbing, has demonstrated a similar kinetic pattern at the fingers as transverse tool gripping (Fuss & Niegl, 2012; Key et al., 2019; Matarazzo, 2015; Samuel et al., 2018; Williams-Hatala et al., 2021). During forelimb locomotor behaviors, the force exerted on the third and fourth digits can be equal to or greater than on the second digit (Amca et al., 2012; Fuss & Niegl, 2012; Quaine et al., 2003; Samuel et al., 2018). When living humans climb rocks, the thumb is not highly loaded (Amca et al., 2012; Sarmiento, 1988). This contrasts with precision gripping tasks, where the thumb is usually the highest or among the highest loaded digit in living humans (Key et al., 2019; Key & Dunmore, 2015; Williams et al., 2012; Williams-Hatala et al., 2018; Williams-Hatala et al., 2021). Climbing and transverse-type grips, such as the cradle grip, may be highly compatible from a kinetic point of view as they both emphasize ulnar-side loading of the hand. Therefore, a reliance on transverse-type grips may have allowed *H. floresiensis*, and potentially other hominins, to improve the functional efficiency of stone tool behavior without highly compromising climbing ability. The upper and lower limb as well as pedal proportions of *H. floresiensis* indicate they would have been efficient and capable climbers (Brown et al., 2004). The trade-off, however, is that the predominant use of transverse-type grips to produce and use stone tools limits the sophistication and mechanical efficiency of these behaviors (Marzke, 1997; Williams-Hatala et al., 2021).

It has been suggested that climbing may have sufficiently differentiated the ecological niche of *H. naledi* from contemporaneous *H. sapiens* such that they could coexist within the same southern African grassland habitat (Dusseldorp & Lombard, 2021). Despite the carpus of *H. naledi* sharing a number of derived features with humans and Neandertals, its curved fingers and ape-like upper limb morphology suggest that climbing and arboreality was an important component of its behavioral repertoire (Feuerriegel et al., 2017; Kivell, 2015). Unfortunately, an undamaged *H. naledi* capitate has yet to be recovered and thus we cannot confidently infer the loading of the proximo-palmar joints; however, there are some notable similarities in the rBV/TV distributions of *H. naledi* and the two *H. floresiensis* capitates. From what is preserved, *H. naledi* showed higher ulnar-side loading of the midcarpal joint. Notably, the proximal portion of the scaphoid subarticular region has mean rBV/TV, clearly distinguishing it from the *H. sapiens*-Neandertal pattern. Mean rBV/TV at the proximal scaphoid is uncommon among our *H. sapiens* sample, with only one individual showing this distribution (UNI-FL 3127, a left capitate from a 19th century male from Tierra del Fuego (Marangoni et al., 2011)). As a continuous band of high rBV/TV from the lunate to the proximal scaphoid subarticular region characterized positive PC1, it is unlikely *H. naledi* would have fallen alongside *H. sapiens* and Neandertals in the PCA. Therefore, despite the more derived aspects of its carpal morphology, *H. naledi* does not appear to resist habitual and/or relatively high loading at the capito-scaphoid articular surface. If *H. naledi* was regularly performing tool behaviors, as parsimony would suggest, the way in which their midcarpal joints were loaded was distinct from that of *H. sapiens* as well as Neandertals but would be reasonably consistent with presumed loading patterns during vertical climbing.

Detecting signals of potential arboreal and/or manipulative behaviors from the proximal capitates of fossils in isolation has limitations, particularly as different behaviors may have elicited similar hand postures and generated comparable loading patterns at the midcarpal joint. For example, the relatively higher ulnar-side loading of the proximal capitate apparent in both *H. naledi* and *H. floresiensis* may indicate frequent climbing, the use of a cradle grip for tool behavior, both, or another as yet unidentified behavior. *A. sediba*, *H. naledi*, and *H. floresiensis* certainly had opportunities to climb within the forests, caves, and rocky outcrops present in their environments (Dusseldorp & Lombard, 2021; Holt et al., 2016; Sutikna et al., 2016). Although studies of rock climbing in living *H. sapiens* provide invaluable kinematic and kinetic data for the behavioral interpretation of fossil taxa, such data are often collected from experiments using artificial climbing walls (e.g., Amca et al., 2012), which may not necessarily replicate the substrates of fossil hominins. Furthermore, there are currently no data on forelimb or hand kinematics of tree climbing in living humans, which potentially loads the hand differently to rock climbing. Hand posture and the concomitant force induced at each digit differ depending on the size and shape of the surface or diameter of support (Amca et al., 2012; Fuss & Niegl, 2012; Neufuss et al., 2017; Sarmiento, 1988). For example, the thumb rarely contacts the substrate during terrestrial knuckle-walking in *Gorilla* (Matarazzo, 2013; Thompson, 2020; Tuttle, 1967), but appears to play an important stabilization role during vertical descent on lianas (Neufuss et al., 2017). Nevertheless, substrate contact is not necessarily associated with high forces, for example, Samuel et al. (2018) found that although the bonobo thumb made contact with the substrate during suspension and climbing, the pressure registered at this location was low or completely absent. Furthermore, the variable phalangeal curvature in these fossil species suggests that the strain induced by climbing may be modulated differently through the hand and wrist compared to living *H. sapiens* (Nguyen et al., 2014; Richmond, 2007; Sarmiento, 1988). Further kinetic analyses or potentially finite element modeling (e.g., Nguyen et al., 2014) on variable taxa and locomotor mode will improve the nuance of predictions and interpretations in future functional adaptation research.

5 | CONCLUSION

The proximal capitates of recent and Pleistocene *H. sapiens* and Neandertals have a distinctive and continuous radio-ulnar band of high trabecular bone volume across the scaphoid, lunate, and hamate subarticular regions that reasonably tracks with the axis of the dart-thrower's motion (DTM). This human/Neandertal pattern is significantly different from that of extant non-human hominids (*Pan*, *Gorilla*, *Pongo*). However, as all extant hominids expressed high relatve bone volume to total volume (rBV/TV) at the capito-lunate joint, it is unclear whether the distinct pattern in *H. sapiens* and Neandertals is a result of: 1) DTM kinematics; or 2) high loading from forceful precision gripping in combination with high loading at the capito-lunate joint as a shared feature of hominid midcarpal biomechanics. *A. sediba* displays a distribution of trabecular bone showing human-like strain at the subarticular capito-scaphoid and capito-lunate regions that was combined with *Pan*-like wrist postures. Both *H. floresiensis* and *H. naledi* had relatively low bone volume at the capito-scaphoid region, suggesting that their midcarpal joints did not experience the same loading patterns as *H. sapiens* and Neandertals. More research is warranted to understand correlations between transverse gripping for tool behavior and vertical climbing, as these two behaviors potentially induce similar kinetic patterns across the wrist, allowing a hominin to improve the efficiency of tool behaviors without highly compromising climbing ability.

AUTHOR CONTRIBUTIONS

Emma E. Bird: Conceptualization (equal); data curation (lead); formal analysis (lead); investigation (lead); methodology (supporting); project administration (lead); visualization (lead); writing – original draft (lead); writing – review and editing (equal). **Tracy L. Kivell:** Conceptualization (equal); methodology (equal); resources (equal); software (equal); supervision (supporting); writing – review and editing (equal). **Christopher J. Dunmore:** Methodology (lead); resources (supporting); software (equal); writing – review and editing (equal). **Matthew W. Tocheri:** Resources (supporting); writing – review and editing (equal). **Matthew M. Skinner:** Conceptualization (equal); methodology

(equal); resources (equal); software (equal); supervision (lead); writing – review and editing (equal).

ACKNOWLEDGMENTS

This research was supported by a 50th Anniversary Research Scholarship, University of Kent, and The Calleva Foundation (Emma E. Bird), FP7 European Research Council Starting Grant #336301, European Union's Horizon 2020 research and innovation programme Grant #819960 and the Max Planck Society (Matthew M. Skinner, Tracy L. Kivell), as well as ERC-SSHRC Visiting Scholar Program and SSHRC Insight Grant #435-2017-1234 (Matthew W. Tocheri). For technical support, we thank S. Bachmann, TU Wien. For providing access to the specimens, we would like to acknowledge: G. Haszprunar, Bavarian State Collection of Zoology; F. Mayer and C. Funk, Berlin Museum für Naturkunde; T. Biers and M. Mirazon Lahr, the Duckworth Collection, University of Cambridge; V. Volpato and K. Krohmann, Frankfurt Senckenberg Museum; B. Groβkopf, Georg-August-University Goettingen, Anthropology Collection; C. Boesch, A. Hildred, the Mary Rose Trust; Max Planck Institute for Evolutionary Anthropology; I. Livne, Powell-Cotton Museum; E. Gilissen and W. Wendelen, Royal Museum for Central Africa; I. Herskovitz, Tel Aviv University; J. Moggi-Cecchi and S. Bortoluzzi, University of Florence; B. Zipfel, University of the Witwatersrand, Johannesburg; M. Teschler-Nicola and R. Muehl, Vienna Natural History Museum; I Made Geria, Pusat Penelitian Arkeologi Nasional (Indonesia). For microCT scanning, we thank R. Freeney, P. Schoenfeld, A. Silvester, K. Smithson, N. Stephens, H. Temming, Z. Tsegai, and A. Winzer.

CONFLICT OF INTEREST STATEMENT

The authors declare no conflicts of interest.

DATA AVAILABILITY STATEMENT

The data that support the findings of this study are available from the corresponding author upon reasonable request.

ORCID

Emma E. Bird https://orcid.org/0000-0001-8232-7485
Tracy L. Kivell https://orcid.org/0000-0001-5087-0897
Christopher J. Dunmore https://orcid.org/0000-0002-8634-9777
Matthew W. Tocheri https://orcid.org/0000-0001-7600-8998
Matthew M. Skinner https://orcid.org/0000-0001-8321-3543

REFERENCES

Amca, A. M., Vigouroux, L., Aritan, S., & Berton, E. (2012). Effect of hold depth and grip technique on maximal finger forces in rock climbing. *Journal of Sports Sciences*, *30*(7), 669–677.

Bachmann, S., Dunmore, C. J., Skinner, M. M., Pahr, D. H., & Synek, A. (2022). A computational framework for canonical holistic morphometric analysis of trabecular bone. *Scientific Reports*, *12*(1), 1–13.

Barak, M. M., Lieberman, D. E., & Hublin, J.-J. (2011). A Wolff in sheep's clothing: Trabecular bone adaptation in response to changes in joint loading orientation. *Bone*, *49*(6), 1141–1151.

Barak, M. M., Lieberman, D. E., Raichlen, D., Pontzer, H., Warrener, A. G., & Hublin, J.-J. (2013). Trabecular evidence for a human-like gait in *Australopithecus africanus*. *PLoS One*, *8*(11), e77687.

Barak, M. M., Sherratt, E., & Lieberman, D. E. (2017). Using principal trabecular orientation to differentiate joint loading orientation in the 3rd metacarpal heads of humans and chimpanzees. *Journal of Human Evolution*, *113*, 173–182.

Bardo, A., Moncel, M.-H., Dunmore, C. J., Kivell, T. L., Pouydebat, E., & Cornette, R. (2020). The implications of thumb movements for Neanderthal and modern human manipulation. *Scientific Reports*, *10*(1), 1–12.

Bird, E. E., Kivell, T. L., & Skinner, M. M. (2021). Cortical and trabecular bone structure of the hominoid capitate. *Journal of Anatomy*, *239*(2), 351–373.

Bird, E. E., Kivell, T. L., & Skinner, M. M. (2022). Patterns of internal bone structure and functional adaptation in the hominoid scaphoid, lunate, and triquetrum. *American Journal of Biological Anthropology*, *177*(2), 266–285.

Brigstocke, G. H. O., Hearnden, A., Holt, C., & Whatling, G. (2014). In-vivo confirmation of the use of the dart thrower's motion during activities of daily living. *The Journal of Hand Surgery*, *39*(4), 373–378.

Brown, P., Sutikna, T., Morwood, M. J., Soejono, R. P., Saptomo, E. W., & Due, R. A. (2004). A new small-bodied hominin from the late Pleistocene of Flores, Indonesia. *Nature*, *431*(7012), 1055–1061.

Brumm, A., Aziz, F., van den Bergh, G. D., Morwood, M. J., Moore, M. W., Kurniawan, I., Hobbs, D. R., & Fullagar, R. (2006). Early stone technology on Flores and its implications for *Homo floresiensis*. *Nature*, *441*(7093), 624–628.

Chirchir, H., Kivell, T. L., Ruff, C. B., Hublin, J. J., Carlson, K. J., Zipfel, B., & Richmond, B. G. (2015). Recent origin of low trabecular bone density in modern humans. *Proceedings of the National Academy of Sciences*, *112*(2), 366–371.

Chirchir, H., Zeininger, A., Nakatsukasa, M., Ketcham, R. A., & Richmond, B. G. (2017). Does trabecular bone structure within the metacarpal heads of primates vary with hand posture? *Comptes Rendus Palevol*, *16*(5–6), 533–544.

Churchill, S. E., Holliday, T. W., Carlson, K. J., Jashashvili, T., Macias, M. E., Mathews, S., Sparling, T. L., Schmid, P., de Ruiter, D. J., & Berger, L. R. (2013). The upper limb of *Australopithecus sediba*. *Science*, *340*(6129), 1233477.

Coppa, A., Grün, R., Stringer, C., Eggins, S., & Vargiu, R. (2005). Newly recognized Pleistocene human teeth from Tabun cave, Israel. *Journal of Human Evolution*, *49*(3), 301–315.

Crisco, J. J., Coburn, J. C., Moore, D. C., Akelman, E., Weiss, A.-P. C., & Wolfe, S. W. (2005). In vivo radiocarpal kinematics and the dart thrower's motion. *The Journal of Bone and Joint Surgery*, *87*(12), 2729–2740.

Dainton, M., & Macho, G. A. (1999). Did knuckle walking evolve twice? *Journal of Human Evolution*, *36*(2), 171–194.

DeSilva, J. M., Carlson, K. J., Claxton, A. G., Harcourt-Smith, W. E., McNutt, E. J., Sylvester, A. D., Walker, C. S., Zipfel, B., Churchill, S. E., & Berger, L. R. (2018). *Australopithecus sediba*: The anatomy of the lower limb skeleton of *Australopithecus sediba*. *Paleo Anthropology*, *2018*, 357–405.

Dirks, P. H., Roberts, E. M., Hilbert-Wolf, H., Kramers, J. D., Hawks, J., Dosseto, A., Duval, M., Elliott, M., Evans, M., & Grün, R. (2017). The age of *Homo naledi* and associated sediments in the Rising Star Cave, South Africa. *Elife*, *6*, e24231.

Doran, D. M. (1996). Comparative positional behavior of the African apes. In W. C. McGrew, L. F. Marchant, & T. Nishida (Eds.), *Great ape societies* (pp. 213–224). Cambridge University Press.

Doran, D. M., & Hunt, K. D. (1994). Comparative locomotor behavior of Chimpanzees and Bonobos: Species and habitat differences. In R. W. M. Wrangham & F. de Waal (Eds.), *Chimpanzee cultures* (p. 93). Harvard University Press.

Dunmore, C. J., Kivell, T. L., Bardo, A., & Skinner, M. M. (2019). Metacarpal trabecular bone varies with distinct hand-positions used in hominid locomotion. *Journal of Anatomy*, *235*(1), 45–66.

Dunmore, C. J., Skinner, M. M., Bardo, A., Berger, L. R., Hublin, J.-J., Pahr, D. H., Rosas, A., Stephens, N. B., & Kivell, T. L. (2020). The

position of *Australopithecus sediba* within fossil hominin hand use diversity. *Nature Ecology & Evolution*, *4*(7), 911–918.

Dunmore, C. J., Wollny, G., & Skinner, M. M. (2018). MIA-clustering: A novel method for segmentation of paleontological material. *PeerJ*, *6*, e4374.

Dusseldorp, G. L., & Lombard, M. (2021). Constraining the likely technological niches of late Middle Pleistocene hominins with *Homo naledi* as case study. *Journal of Archaeological Method and Theory*, *28*(1), 11–52.

Edirisinghe, Y., Troupis, J., Patel, M., Smith, J., & Crossett, M. (2014). Dynamic motion analysis of dart throwers motion visualized through computerized tomography and calculation of the axis of rotation. *The Journal of Hand Surgery (European Volume)*, *39*(4), 364–372.

Fajardo, R. J., & Müller, R. (2001). Three-dimensional analysis of nonhuman primate trabecular architecture using micro-computed tomography. *American Journal of Physical Anthropology*, *115*(4), 327–336.

Feuerriegel, E. M., Green, D. J., Walker, C. S., Schmid, P., Hawks, J., Berger, L. R., & Churchill, S. E. (2017). The upper limb of *Homo naledi*. *Journal of Human Evolution*, *104*, 155–173.

Formicola, V., Pettitt, P., & DelLucchese, A. (2004). A direct AMS radiocarbon date on the Barma Grande 6 Upper Paleolithic skeleton. *Current Anthropology*, *45*(1), 114–118.

Fuss, F. K., & Niegl, G. (2012). Finger load distribution in different types of climbing grips. *Sports Technology*, *5*(3–4), 151–155.

Garcia-Elias, M., Alomar Serrallach, X., & Monill Serra, J. (2014). Dart-throwing motion in patients with scapholunate instability: A dynamic four-dimensional computed tomography study. *The Journal of Hand Surgery (European Volume)*, *39*(4), 346–352.

Georgiou, L., Dunmore, C. J., Bardo, A., Buck, L. T., Hublin, J. J., Pahr, D. H., Stratford, D., Synek, A., Kivell, T. L., & Skinner, M. M. (2020). Evidence for habitual climbing in a Pleistocene hominin in South Africa. *Proceedings of the National Academy of Sciences*, *117*(15), 8416–8423.

Griffin, N. L., D'Août, K., Ryan, T. M., Richmond, B. G., Ketcham, R. A., & Postnov, A. (2010). Comparative forefoot trabecular bone architecture in extant hominids. *Journal of Human Evolution*, *59*(2), 202–213.

Gross, T., Kivell, T. L., Skinner, M. M., Nguyen, H., & Pahr, D. H. (2014). Holistic analysis of bone. *Palaeontologia Electronica*, *17*(3), 1.

Hawks, J., Elliott, M., Schmid, P., Churchill, S. E., de Ruiter, D. J., Roberts, E. M., Hilbert-Wolf, H., Garvin, H. M., Williams, S. A., & Delezene, L. K. (2017). New fossil remains of *Homo naledi* from the Lesedi Chamber, South Africa. *Elife*, *6*, e24232.

Henry, A. G., Ungar, P. S., Passey, B. H., Sponheimer, M., Rossouw, L., Bamford, M., Sandberg, P., de Ruiter, D. J., & Berger, L. (2012). The diet of *Australopithecus sediba*. *Nature*, *487*(7405), 90–93.

Hershkovitz, I., Speirs, M. S., Frayer, D., Nadel, D., Wish-Baratz, S., & Arensburg, B. (1995). Ohalo II H2: A 19,000-year-old skeleton from a water-logged site at the Sea of Galilee, Israel. *American Journal of Physical Anthropology*, *96*(3), 215–234.

Hervé, M. (2021). RVAideMemoire: Testing and plotting procedures for biostatistics. R package version (version 0.9-80). https://cran.r-project.org/web/packages/RVAideMemoire/index.html.

Higham, T., Douka, K., Wood, R., Ramsey, C. B., Brock, F., Basell, L., Camps, M., Arrizabalaga, A., Baena, J., & Barroso-Ruíz, C. (2014). The timing and spatiotemporal patterning of Neanderthal disappearance. *Nature*, *512*(7514), 306–309.

Holt, E., Dirks, P., Placzek, C., & Berger, L. (2016). The stable isotope setting of *Australopithecus sediba* at Malapa, South Africa. *South African Journal of Science*, *112*(7–8), 1–9.

Hughes, J. M., Gaffney-Stomberg, E., Guerriere, K. I., Taylor, K. M., Popp, K. L., Xu, C., Unnikrishnan, G., Staab, J. S., Matheny, R. W., Jr., & McClung, J. P. (2018). Changes in tibial bone microarchitecture in female recruits in response to 8 weeks of US Army Basic Combat Training. *Bone*, *113*, 9–16.

Jenkins, F. A., & Fleagle, J. G. (1975). Knuckle-walking and the functional anatomy of the wrists in living apes. In R. Tuttle (Ed.), *Primate functional morphology and evolution* (pp. 213–227). Mouton.

Karakostis, F. A., Hotz, G., Tourloukis, V., & Harvati, K. (2018). Evidence for precision grasping in Neandertal daily activities. *Science Advances*, *4*(9), eaat2369.

Kassambara, A., & Mundt, F. (2020). Factoextra: Extract and visualize the results of multivariate data analyses. R package version (Version 1.0.7). https://cran.r-project.org/web/packages/factoextra/index.html.

Kaufman-Cohen, Y., Friedman, J., Levanon, Y., Jacobi, G., Doron, N., & Portnoy, S. (2018). Wrist plane of motion and range during daily activities. *American Journal of Occupational Therapy*, *72*(6), 7206205080.

Key, A., & Dunmore, C. J. (2015). The evolution of the hominin thumb and the influence exerted by the non-dominant hand during stone tool production. *Journal of Human Evolution*, *78*, 60–69.

Key, A., Dunmore, C. J., & Marzke, M. W. (2019). The unexpected importance of the fifth digit during stone tool production. *Scientific Reports*, *9*(1), 1–8.

Key, A., Farr, I., Hunter, R., & Winter, S. L. (2020). Muscle recruitment and stone tool use ergonomics across three million years of Palaeolithic technological transitions. *Journal of Human Evolution*, *144*, 102796.

Key, A., Merritt, S. R., & Kivell, T. L. (2018). Hand grip diversity and frequency during the use of Lower Palaeolithic stone cutting-tools. *Journal of Human Evolution*, *125*, 137–158.

Kivell, T. L. (2015). Evidence in hand: Recent discoveries and the early evolution of human manual manipulation. *Philosophical Transactions of the Royal Society B: Biological Sciences*, *370*(1682), 20150105.

Kivell, T. L. (2016). A review of trabecular bone functional adaptation: What have we learned from trabecular analyses in extant hominoids and what can we apply to fossils? *Journal of Anatomy*, *228*(4), 569–594.

Kivell, T. L., Churchill, S. E., Kibii, J. M., Schmid, P., & Berger, L. R. (2018). The hand of Australopithecus sediba. *Paleo Anthropology*, 282–333.

Kivell, T. L., Deane, A. S., Tocheri, M. W., Orr, C. M., Schmid, P., Hawks, J., Berger, L. R., & Churchill, S. E. (2015). The hand of *Homo naledi*. *Nature Communications*, *6*, 8431.

Kivell, T. L., Kibii, J. M., Churchill, S. E., Schmid, P., & Berger, L. R. (2011). *Australopithecus sediba* hand demonstrates mosaic evolution of locomotor and manipulative abilities. *Science*, *333*(6048), 1411–1417.

Kivell, T. L., & Schmitt, D. (2009). Independent evolution of knuckle-walking in African apes shows that humans did not evolve from a knuckle-walking ancestor. *Proceedings of the National Academy of Sciences*, *106*(34), 14241–14246.

Komza, K., & Skinner, M. M. (2019). First metatarsal trabecular bone structure in extant hominoids and Swartkrans hominins. *Journal of Human Evolution*, *131*, 1–21.

Larson, S. G., Jungers, W. L., Tocheri, M. W., Orr, C. M., Morwood, M. J., Sutikna, T., Awe, R. D., & Djubiantono, T. (2009). Descriptions of the upper limb skeleton of *Homo floresiensis*. *Journal of Human Evolution*, *57*(5), 555–570.

Lewis, O. J. (1989). *Functional morphology of the evolving hand and foot*. Oxford University Press.

Lieberman, D. E. (1997). Making behavioral and phylogenetic inferences from hominid fossils: Considering the developmental influence of mechanical forces. *Annual Review of Anthropology*, *26*(1), 185–210.

Marangoni, A., Belli, M. L., Caramelli, D., Moggi Cecchi, J., Zavattaro, M., & Manzi, G. (2011). Tierra del Fuego, its ancient inhabitants, and the collections of skeletal remains in the Museum of Anthropology of Florence and Rome. *Museologia Scientifica*, *5*(1–2), 88–96.

Marzke, M. W. (1997). Precision grips, hand morphology, and tools. *American Journal of Physical Anthropology*, *102*(1), 91–110.

Marzke, M. W. (2013). Tool making, hand morphology and fossil hominins. *Philosophical Transactions of the Royal Society B: Biological Sciences*, *368*(1630), 1–8.

Marzke, M. W., Wullstein, K., & Viegas, S. F. (1992). Evolution of the power ("squeeze") grip and its morphological correlates in hominids. *American Journal of Physical Anthropology*, *89*(3), 283–298.

Matarazzo, S. (2013). Manual pressure distribution patterns of knuckle-walking apes. *American Journal of Physical Anthropology*, *152*(1), 44–50.

Matarazzo, S. (2015). Trabecular architecture of the manual elements reflects locomotor patterns in primates. *PLoS One*, *10*(3), e0120436.

Moore, M. W., & Brumm, A. (2009). *Homo floresiensis* and the African Oldowan. In E. Hovers & D. R. Braun (Eds.), *Interdisciplinary approaches to the Oldowan* (pp. 61–69). Springer.

Napier, J. (1962). The evolution of the hand. *Scientific American*, *207*(6), 56–65.

Neufuss, J., Robbins, M. M., Baeumer, J., Humle, T., & Kivell, T. L. (2017). Comparison of hand use and forelimb posture during vertical climbing in mountain gorillas (*Gorilla beringei beringei*) and chimpanzees (*Pan troglodytes*). *American Journal of Physical Anthropology*, *164*(4), 651–664.

Nguyen, N. H., Pahr, D. H., Gross, T., Skinner, M. M., & Kivell, T. L. (2014). Micro-finite element (μFE) modeling of the siamang (*Symphalangus syndactylus*) third proximal phalanx: The functional role of curvature and the flexor sheath ridge. *Journal of Human Evolution*, *67*, 60–75.

Niewoehner, W. A., Weaver, A. H., & Trinkaus, E. (1997). Neandertal capitate-metacarpal articular morphology. *American Journal of Physical Anthropology*, *103*(2), 219–233.

Oksanen, J., Blanchet, F. G., Kindt, R., Legendre, P., Minchin, P., O'hara, R., Simpson, G., Solymos, P., Stevens, M. H. H., & Wagner, H. (2021). Community ecology package. In R package version (Version 2.5-7). https://cran.r-project.org/web/packages/vegan/index.html.

Orr, C. M. (2017). Locomotor hand postures, carpal kinematics during wrist extension, and associated morphology in anthropoid primates. *The Anatomical Record*, *300*(2), 382–401.

Orr, C. M., Tocheri, M. W., Burnett, S. E., Awe, R. D., Saptomo, E. W., Sutikna, T., Wasisto, S., Morwood, M. J., & Jungers, W. L. (2013). New wrist bones of *Homo floresiensis* from Liang Bua (Flores, Indonesia). *Journal of Human Evolution*, *64*(2), 109–129.

Pickering, R., Dirks, P. H., Jinnah, Z., de Ruiter, D. J., Churchill, S. E., Herries, A. I., Woodhead, J. D., Hellstrom, J. C., & Berger, L. R. (2011). *Australopithecus sediba* at 1.977 Ma and implications for the origins of the genus *Homo*. *Science*, *333*(6048), 1421–1423.

Pontzer, H., Lieberman, D. E., Momin, E., Devlin, M. J., Polk, J., Hallgrimsson, B., & Cooper, D. (2006). Trabecular bone in the bird knee responds with high sensitivity to changes in load orientation. *Journal of Experimental Biology*, *209*(1), 57–65.

Quaine, F., Vigouroux, L., & Martin, L. (2003). Effect of simulated rock climbing finger postures on force sharing among the fingers. *Clinical Biomechanics*, *18*(5), 385–388.

R Core Team. (2013). R: A language and environment for statistical computing (Version 4.1.0).

Ragni, A. J. (2020). Trabecular architecture of the capitate and third metacarpal through ontogeny in chimpanzees (*Pan troglodytes*) and gorillas (*Gorilla gorilla*). *Journal of Human Evolution*, *138*, 102702.

Reina, N., Cavaignac, E., Trousdale, W. H., Laffosse, J. M., & Braga, J. (2017). Laterality and grip strength influence hand bone microarchitecture in modern humans, an HR p QCT study. *Journal of Anatomy*, *230*(6), 796–804.

Remis, M. J. (1999). Tree structure and sex differences in arboreality among western lowland gorillas (*Gorilla gorilla gorilla*) at Bai Hokou, Central African Republic. *Primates*, *40*(2), 383–396.

Richmond, B. G. (2007). Biomechanics of phalangeal curvature. *Journal of Human Evolution*, *53*(6), 678–690.

Richmond, B. G., Begun, D. R., & Strait, D. S. (2001). Origin of human bipedalism: The knuckle-walking hypothesis revisited. *American Journal of Physical Anthropology*, *116*(S33), 70–105.

Ryan, T. M., & Ketcham, R. A. (2002). Femoral head trabecular bone structure in two omomyid primates. *Journal of Human Evolution*, *43*(2), 241–263.

Ryan, T. M., & Shaw, C. N. (2012). Unique suites of trabecular bone features characterize locomotor behavior in human and non-human anthropoid primates. *PLoS One*, *7*(7), e41037.

Samuel, D. S., Nauwelaerts, S., Stevens, J. M., & Kivell, T. L. (2018). Hand pressures during arboreal locomotion in captive bonobos (*Pan paniscus*). *Journal of Experimental Biology*, *221*(8), e170910.

Sarmiento, E. E. (1988). Anatomy of the hominoid wrist joint: Its evolutionary and functional implications. *International Journal of Primatology*, *9*(4), 281–345.

Schilling, A. M., Tofanelli, S., Hublin, J. J., & Kivell, T. L. (2014). Trabecular bone structure in the primate wrist. *Journal of Morphology*, *275*(5), 572–585.

Schwarcz, H., Buhay, W., Grün, R., Valladas, H., Tchernov, E., Bar-Yosef, O., & Vandermeersch, B. (1989). ESR dating of the Neanderthal site, Kebara cave, Israel. *Journal of Archaeological Science*, *16*(6), 653–659.

Skinner, M. M., Stephens, N. B., Tsegai, Z. J., Foote, A. C., Nguyen, N. H., Gross, T., Pahr, D. H., Hublin, J. J., & Kivell, T. L. (2015). Human-like hand use in *Australopithecus africanus*. *Science*, *347*(6220), 395–399.

Soetaert, K. (2021). plot3D: Tools for plotting 3-D and 2-D data. R package version (Version 1.4). https://cran.r-project.org/web/packages/plot3D/index.html.

Sparacello, V. S., Rossi, S., Pettitt, P., Roberts, C., Salvatore, J., & Formicola, V. (2018). New insights on final Epigravettian funerary behaviour at Arene Candide cave (Western Liguria, Italy) from osteological and spatial analysis of secondary bone deposits. *Journal of Anthropological Sciences*, *96*, 1–24.

Steiner, L., Synek, A., & Pahr, D. H. (2021). Femoral strength can be predicted from 2D projections using a 3D statistical deformation and texture model with finite element analysis. *Medical Engineering & Physics*, *93*, 72–82.

Stephens, N. B., Kivell, T. L., Pahr, D. H., Hublin, J.-J., & Skinner, M. M. (2018). Trabecular bone patterning across the human hand. *Journal of Human Evolution*, *123*, 1–23.

Su, A., & Carlson, K. J. (2017). Comparative analysis of trabecular bone structure and orientation in South African hominin tali. *Journal of Human Evolution*, *106*, 1–18.

Sutikna, T., Tocheri, M. W., Morwood, M. J., Saptomo, E. W., Awe, R. D., Wasisto, S., Westaway, K. E., Aubert, M., Li, B., & Zhao, J.-X. (2016). Revised stratigraphy and chronology for *Homo floresiensis* at Liang Bua in Indonesia. *Nature*, *532*(7599), 366–369.

Thompson, N. E. (2020). The biomechanics of knuckle-walking: 3-D kinematics of the chimpanzee and macaque wrist, hand and fingers. *Journal of Experimental Biology*, *223*(14), jeb224360.

Tocheri, M. W., Orr, C. M., Jacofsky, M. C., & Marzke, M. W. (2008). The evolutionary history of the hominin hand since the last common ancestor of *Pan* and *Homo*. *Journal of Anatomy*, *212*(4), 544–562.

Tocheri, M. W., Orr, C. M., Larson, S. G., Sutikna, T., Jatmiko, Saptomo, E. W., Due, R. A., Djubiantono, T., Morwood, M. J., & Jungers, W. L. (2007). The primitive wrist of *Homo floresiensis* and its implications for hominin evolution. *Science*, *317*(5845), 1743–1745.

Tocheri, M. W., Razdan, A., Williams, R. C., & Marzke, M. W. (2005). A 3D quantitative comparison of trapezium and trapezoid relative articular and nonarticular surface areas in modern humans and great apes. *Journal of Human Evolution*, *49*(5), 570–586.

Tsegai, Z. J., Kivell, T. L., Gross, T., Nguyen, N. H., Pahr, D. H., Smaers, J. B., & Skinner, M. M. (2013). Trabecular bone structure correlates with hand posture and use in hominoids. *PLoS One*, *8*(11), e78781.

Tsegai, Z. J., Skinner, M. M., Pahr, D. H., Hublin, J. J., & Kivell, T. L. (2018). Systemic patterns of trabecular bone across the human and chimpanzee skeleton. *Journal of Anatomy*, *232*(4), 641–656.

Tuttle, R. H. (1967). Knuckle-walking and the evolution of hominoid hands. *American Journal of Physical Anthropology*, *26*(2), 171–206.

Valladas, H., Mercier, N., Froget, L., Hovers, E., Joron, J.-L., Kimbel, W. H., & Rak, Y. (1999). TL dates for the Neanderthal site of the Amud Cave, Israel. *Journal of Archaeological Science*, *26*(3), 259–268.

Ward, C. V. (2002). Interpreting the posture and locomotion of *Australopithecus afarensis*: Where do we stand? *American Journal of Physical Anthropology*, *119*(S35), 185–215.

Williams, E. M., Gordon, A. D., & Richmond, B. G. (2010). Upper limb kinematics and the role of the wrist during stone tool production. *American Journal of Physical Anthropology*, *143*(1), 134–145.

Williams, E. M., Gordon, A. D., & Richmond, B. G. (2012). Hand pressure distribution during Oldowan stone tool production. *Journal of Human Evolution*, *62*(4), 520–532.

Williams, E. M., Gordon, A. D., & Richmond, B. G. (2014). Biomechanical strategies for accuracy and force generation during stone tool production. *Journal of Human Evolution*, *72*, 52–63.

Williams-Hatala, E. M., Hatala, K. G., Gordon, M., Key, A., Kasper, M., & Kivell, T. L. (2018). The manual pressures of stone tool behaviors and their implications for the evolution of the human hand. *Journal of Human Evolution*, *119*, 14–26.

Williams-Hatala, E. M., Hatala, K. G., Key, A., Dunmore, C. J., Kasper, M., Gordon, M., & Kivell, T. L. (2021). Kinetics of stone tool production among novice and expert tool makers. *American Journal of Physical Anthropology*, *174*(4), 714–727.

Wolfe, S. W., Crisco, J. J., Orr, C. M., & Marzke, M. W. (2006). The dart-throwing motion of the wrist: Is it unique to humans? *The Journal of Hand Surgery*, *31*(9), 1429–1437.

Wunderlich, R. E., & Jungers, W. L. (2009). Manual digital pressures during knuckle-walking in chimpanzees (*Pan troglodytes*). *American Journal of Physical Anthropology*, *139*(3), 394–403.

SUPPORTING INFORMATION

Additional supporting information can be found online in the Supporting Information section at the end of this article.

How to cite this article: Bird, E. E., Kivell, T. L., Dunmore, C. J., Tocheri, M. W., & Skinner, M. M. (2023). Trabecular bone structure of the proximal capitate in extant hominids and fossil hominins with implications for midcarpal joint loading and the dart-thrower's motion. *American Journal of Biological Anthropology*, 1–16. https://doi.org/10.1002/ajpa.24824